JMEPEG (2019) 28:6626–6637
https://doi.org/10.1007/s11665-019-04431-2

1059-9495/$19.00

Strain-Rate Effect and Constitutive Models for Q550 High-Strength Structural Steel

Hua Yang, Xiaoqiang Yang, Amit H. Varma, and Yong Zhu

(Submitted May 30, 2019; in revised form October 9, 2019; published online November 7, 2019)

High-strength structural steel is the tendency in modern construction practice. In this study, quasi-static tension tests and dynamic tests for Q550 with strain rate from 0.00025 to 3831 s^{-1} were conducted. The results showed that Q550 is dependent on the strain rate, keeping the flow stress increased as the strain rate increases, while Q550 has lower strain-rate sensitivity of flow stress than that of normal mild steel. Based on the experimental data, a proper constant for the key parameter, *C*, in Johnson–Cook model (J–C) was suggested. Then, a modified J–C model based on a rate-dependent parameter $C(\dot{\varepsilon})$ was recommended to consider the influence of strain-rate effect. New constants of *D* and *p* governing the dynamic response of steel in the Cowper–Symonds (C–S) model were also suggested. The C–S model and J–C models with suggested constants provided in the paper were proven to have acceptable prediction accuracy for the dynamic increase factor of Q550. These results may be applied to study the dynamical properties of Q550 and related structural components for future engineering applications.

Keywords dynamic constitutive models, high strain rate, high-strength structural steel, Q550, split Hopkinson pressure bar

1. Introduction

High-strength structural steel (HSSS) is a type of steel whose yield stress is not less than 460 MPa for building structures (Ref 1). Replacing the ordinary mild steel, the application of HSSS in those grand engineering structures brings benefits—reducing total steel consumption, enlarging the non-structural area, and environmental protection. Over the past decades, HSSS has been progressively used in civil construction practice (Ref 2), such as Sony Center (Berlin, 690 MPa), Latitude Building (Sydney, 690 MPa), and Lotte World Tower (Seoul, 800 MPa). Compared with normal-strength steels, HSSS exhibits a similar elastic stage, but after yielding, its ability to deform during the plastic stage is different, i.e., no visible yield plateau, higher yield-to-tensile stress ratio and lower elongation (Ref 3). Except for static properties, its dynamic properties subjected to typical dynamic loads have not been clarified mainly due to a lack of theoretical studies and practical applications. As a result, it may be unsuitable for applying the design and research methods of conventional mild steels to study HSSS directly, especially for dynamical analysis.

In recent years, a series of related studies regarding HSSS were gradually conducted by researchers. In 2011, the welding performance and cracking sensibility of weld metal for Q550 and Q690 high-strength steels were studied by Zhang et al. (Ref 4). From then on, the fatigue behavior (Ref 5, 6), welding properties (Ref 7), low-temperature resistance (Ref 8), elevated temperature (Ref 9), and post-fire mechanical properties (Ref 1, 10, 11) of HSSS (460 and 690 MPa) have been tested and analyzed by scholars. Based on researching material properties, researchers began to conduct studies on component performance. In 2012, welded columns made of 460 MPa high-strength steel under axial load had been experimentally studied and numerically analyzed by Ban et al. (Ref 12) and Wang et al. (Ref 13). Later, the compressive behavior of Q690 welded box- and H-columns was investigated experimentally and numerically by Li et al. (Ref 14, 15). In 2017, Wang et al. (Ref 16) studied the axial behavior of high-strength steel prestressed trusses (S460 and S690).

As known, accidental disasters (e.g., vehicle impact, explosion, and progressive collapse) for building structures and infrastructures were regularly reported, which caused enormous loss of life and economic damage, especially for those grand constructions. Therefore, as the basis of conducting studies of structural components and frame systems exposed to such dynamic loadings, the dynamical properties of structural steels are essential, and the strain-rate effect needs to be clarified. From the middle of the twentieth century, studies (Ref 17-20) on the rate-dependence of mild structural steels with normal strength under rapidly applied loadings have been conducted. Recently, several types of modern constructional steels have been investigated to obtain their dynamical stress–strain curves. In 2010, Yu et al. (Ref 21) conducted experiments to study the strain-rate effect of Q345 steel subjected to elevated temperature, and the test results illustrated that Q345 is strain-rate

Hua Yang, Key Lab of Structures Dynamic Behavior and Control of the Ministry of Education, Harbin Institute of Technology, Harbin 150090, China; and School of Civil Engineering, Harbin Institute of Technology, Room 207, Huanghe Road #73, Nangang District, Harbin 150090 Heilongjiang Province, China; **Xiaoqiang Yang**, School of Civil Engineering, Harbin Institute of Technology, Room 207, Huanghe Road #73, Nangang District, Harbin 150090 Heilongjiang Province, China; and Lyles School of Civil Engineering, Purdue University, West Lafayette, IN 47907; **Amit H. Varma**, Lyles School of Civil Engineering, Purdue University, West Lafayette, IN 47907; and **Yong Zhu**, School of Civil Engineering, Harbin Institute of Technology, Room 207, Huanghe Road #73, Nangang District, Harbin 150090 Heilongjiang Province, China. Contact e-mails: yanghua@hit.edu.cn, yangxiaoqiang2016@hit.edu.cn, ahvarma@purdue.edu, and zhuyong@stu.hit.edu.cn.

dependent at room and high temperature. In 2015, a comprehensive study was conducted by Mirmomeni et al. (Ref 22) to investigate the fire behavior of Grade 350 steel after dynamic tension tests with the strain rate up to 10 s^{-1}. Subsequently, in 2016, the dynamic tension behaviors of S355 at intermediate strain rates (5-25 s^{-1}) using a hydropneumatic machine and at high strain rates (350-850 s^{-1}) by a modified Split Hopkinson Tensile Bar (SHTB) were studied by Forni et al. (Ref 23). A series of investigations for Q345 and Q420 steels at medium strain rates using a rapid tension tester were conducted by Chen et al. (Ref 24, 25), and relative rate-dependent models that improve prediction precision of dynamic responses were developed. A recent study on rate-dependent constitutive models for S690 was reported by Yang et al. (Ref 26), showing the considerable difference in the strain-rate effect between S690 and normal-strength steels.

Though the strain-rate effect of normal-strength steels has been extensively researched, the studies regarding high-strength steels are still insufficient. These studies have mainly focused on the DIF of yield and tensile strength based on the tests of high-strength reinforcing bars and steels (Ref 26-31). When using the equations established before (Ref 26-31) to predict the DIF for some specific strengths (460, 550, and 690 MPa), the prediction values are quite different compared with each other, as shown in Fig. 1. As a result, it may cause errors if these equations are applied to the analysis of HSSS or related structural components directly. Therefore, it is necessary to conduct a systematic investigation for HSSS to clarify the strain-rate effect and work out complete material constitutive models for further analyses.

This paper presents an experimental investigation on the dynamical properties of Q550 steel at a wide range of strain rates, which is a grade of HSSS in China with close mechanical properties to S550 in EN 1993-1-12 (yield strength is not less than 550 MPa; tensile strength is 640-820 MPa; and elongation should not be less than 16%). In this study, a universal electromechanical testing machine and Split Hopkinson Pressure Bar (SHPB) were employed to obtain the strain–stress curves of Q550 for quasi-static and dynamic tests, respectively. Based on the test results, the strain-rate effect of flow stress has been discussed. Three constitutive models for Q550 at various strain rates were developed, which may be used to predict the dynamic material behaviors under quick loadings precisely.

2. Experimental Program

2.1 Material and Specimens

Q550GJC produced by Wuhan Iron and Steel (Group) Company, China, was studied in this paper, of which chemical composition is shown in Table 1. All specimens were cut from the same commercial hot rolled steel plate. The geometry of quasi-static tension specimens was adopted according to ISO 6892-1:2016 and ISO 377:2013, as shown in Fig. 2(a). For dynamical SHPB tests, the diameter and length of cylindrical specimens were 8 mm and 4 mm, respectively, as shown in Fig. 2(b).

2.2 Experimental Setup

2.2.1 Tension Tests. All quasi-static tension tests were carried out at room temperature by Shimadzu AG–X Plus 250kN, as shown in Fig. 3. The tensile force and extension used to calculate the engineering stress–strain curves were recorded by a force sensor and an extensometer, respectively. The Young's modulus and Poisson's ratio of Q550 were calculated by longitudinal and transverse strains at the elastic period, which were recorded by strain gauges stuck onto the middle surface at both sides of specimens. The crosshead separation rate was 0.9 mm/min during the test, so the strain rate was 0.00025 s^{-1} (the parallel length is 60 mm) for the quasi-static tests. Three repeated experiments were performed, respectively, to guarantee the reliability and consistency of the test results.

2.2.2 Dynamic Experiments. There are several methods to investigate the mechanical behaviors of materials at medium and high strain rates, such as high-speed electrohydraulic testing machine, Hopkinson bar system, and gas gun. In this paper, an SHPB tester has been adopted to investigate the Q550 at high strain rates. The SHPB system is shown in Fig. 4, which consists of a striking bar, an incident bar, and a transmission bar. Additionally, a gas emitting device, an energy absorption setup, and a data recording system are also included. All the components are on the same axis by being installed on a horizontal guide rail. The cylindrical specimen sandwiched between the incident bar and transmission bar is lubricated by applying petroleum jelly on each interface to reduce the

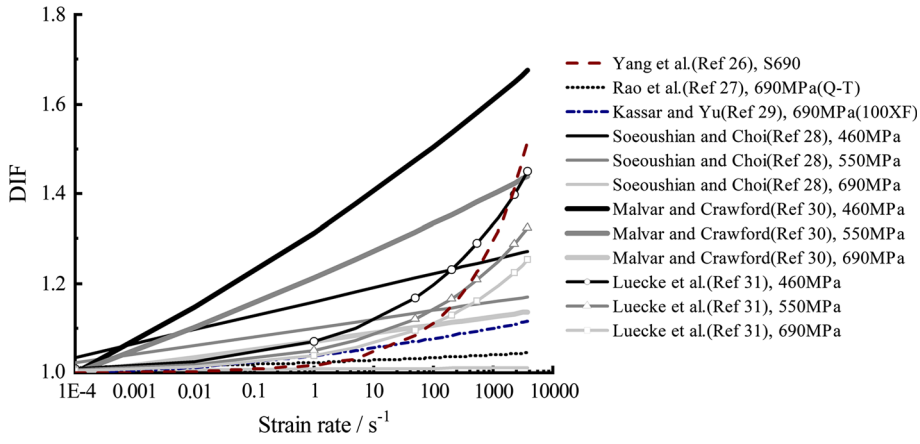

Fig. 1 Relationships of DIF vs. strain rate for high-strength steels based on previous researches

Table 1 Chemical composition of Q550GJC steel (in wt.%)

C	Si	Mn	S	P	N	Ni	Cr	Mo	Cu	V	Nb	Ti
0.062	0.27	1.8	0.001	0.013	0.004	0.23	0.25	0.23	0.045	0.003	0.07	0.015

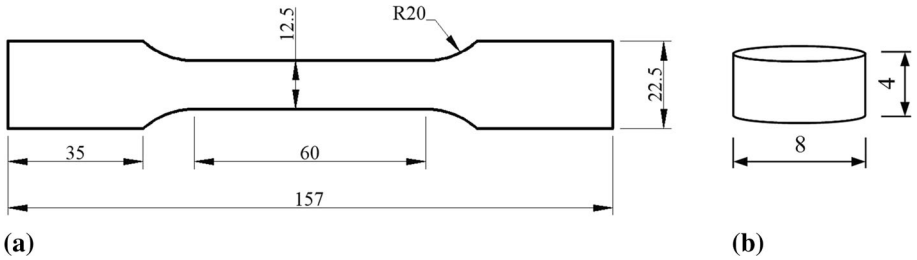

Fig. 2 Geometry of test specimens: (a) quasi-static tension and (b) SHPB (unit: mm)

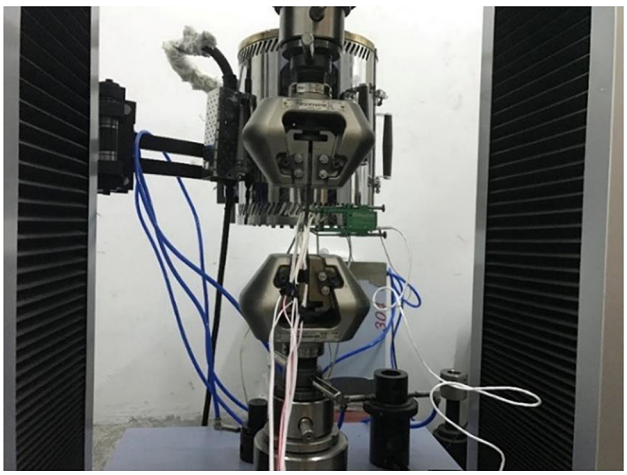

Fig. 3 Universal electromechanical testing machine

influence of friction. In this paper, the incident and transmission bars are both 1200 mm in length and the strike bar is 200 mm, with 16 mm in diameter for all of them. These bars are all fabricated from high-strength alloy steels, whose wave speed is about 5000 m/s (ρ = 7850 kg/m^3 and E = 200 GPa).

During the tests, the pneumatic valve was controlled by the computer system to control the nitrogen gas cylinder inflating the gas cabin to a specified pressure. After pressing the "launch" button, the strike bar would be propelled to impact the incident bar from the gas cabin by the high-pressure gas. The striking velocity was recorded by the laser velocimeter when the strike bar was reaching the incident bar. As the striking bar arrived at the incident bar, an elastic incident wave (ε_I) was generated and propagated forward. Once ε_I reached the specimen, the specimen deformed, and the wave reflected on the interface generating a reflected wave (ε_R). Then, a transmission wave (ε_T) passed to the transmission bar from the specimen and propagated through that. During the whole test, all these bars remained elastic and the time histories of ε_I, ε_R, and ε_T were recorded by the strain gauges with a high-speed digital storing oscilloscope.

In accordance with the data of strain waves, the engineering stress (σ_{eng}), engineering strain (ε_{eng}), and strain rate ($\dot{\varepsilon}$) in the function of time t could be calculated using the two-wave method through Eq 1.

$$\begin{cases} \sigma_{eng}(t) = \frac{EA_0}{A_s}\varepsilon_T(t) \\ \varepsilon_{eng}(t) = -\frac{2C_0}{L}\int_0^t \varepsilon_R(t)\mathrm{d}t \\ \dot{\varepsilon}(t) = -\frac{2C_0}{L}\varepsilon_R(t) \end{cases} \quad \text{(Eq 1)}$$

where A_0 and E represent the cross-sectional area and young's modulus, respectively, and C_0 represents the strain wave speed (5000 m/s) of the incident/transmission bar. L and A_s are the length and cross-sectional area of the specimen, respectively. The true stress (σ_{true}) and true strain (ε_{true}) can be derived from the engineering stress and engineering strain by Eq 2.

$$\begin{cases} \sigma_{true} = \sigma_{eng}(1+\varepsilon_{eng}) \\ \varepsilon_{true} = ln(1+\varepsilon_{eng}) \end{cases} \quad \text{(Eq 2)}$$

To get various strain rates, SHPB steel specimens were tested at five impact velocities: 12.6, 17.2, 23.6, 28.4, and 32.7 m/s. Three repeated experiments were conducted, respectively, for Q550 steel at each impact velocity to guarantee the reliability of the tests.

3. Results and Discussion

3.1 Experimental Results

3.1.1 Quasi-Static Tensile Tests. The tensile properties of Q550 high-strength steel under uniaxial quasi-static tension tests at room temperature are summarized in Table 2, and all tensile performance indexes met the demands for HSSS in the design of steel structures according to EN 1993-1-12. A typical

(a)

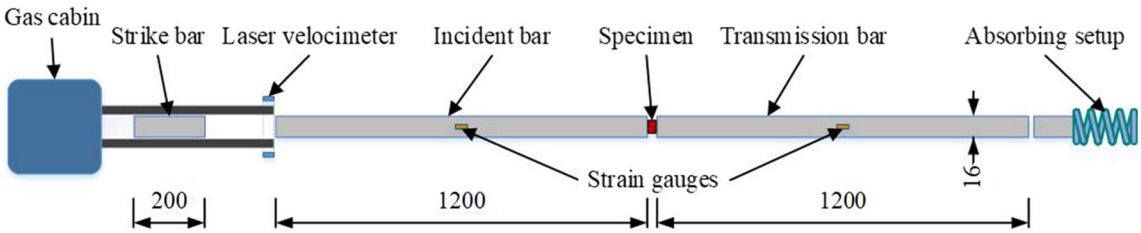

(b)

Fig. 4 Split Hopkinson Pressure Bar (SHPB) testing system: (a) SHPB device and (b) specific dimensions and details (unit: mm)

Table 2 Tensile properties of Q550 under uniaxial quasi-static tension tests

Grade	Yield stress $\sigma_{0.2}$, N/mm^2	Tensile stress σ_u, N/mm^2	Young's modulus E, N/mm^2	Poisson's ratio	Elongation, %
Q550	623	779	206,000	0.281	16
	617	770	202,000	0.291	17
	632	784	201,000	0.280	17
Average	624	778	203,000	0.284	17

shape of the stress–strain curve of Q550 was recorded as most of HSSS without the yield platform showing an initial linear elastic part, immediately followed by the strain strengthening when plastic strain began to grow. After necking of the steel specimen, the engineering stress illustrated a big drop with the increase in engineering strain until fracture occurred. As Q550 did not display a visible yield phenomenon, the proof stress (at 0.2% plastic strain) was chosen as the yield stress of Q550 in this study. The three repeated engineering stress–strain curves showed high consistency, as shown in Fig. 5.

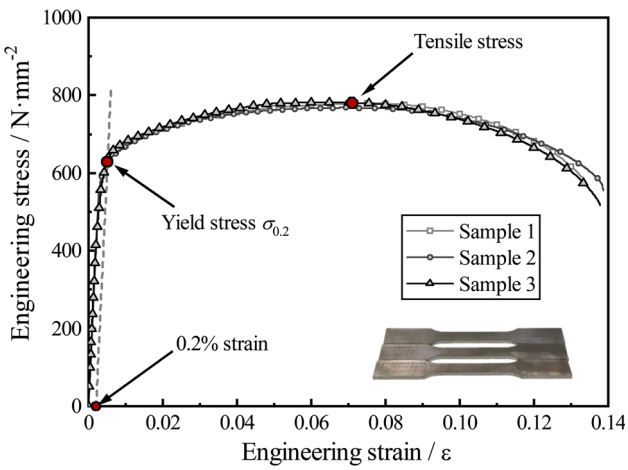

Fig. 5 Engineering stress–strain curve of Q550 under uniaxial quasi-static tension test

3.1.2 SHPB Tests.

a. Verification of stress equilibrium

According to the theory of the one-dimensional elastic wave, the stress uniformity within the specimen during the SHPB tests is essential for the accuracy of the test results. For an SHPB test, the typical ε_I, ε_R, and ε_T were recorded from the incident bar and transmission bar at an impact velocity of 23.6 m/s, as shown in Fig. 6(a). It can be noted that when the starting points of these three waves were moved to the same time, ε_T was generally close to the time history of $\varepsilon_I + \varepsilon_R$, as shown in Fig. 6(b), although $\varepsilon_I + \varepsilon_R$ had a little vibration at the beginning of tests. The similar results have been obtained for other terms at different impact velocities. The forces on the front and back of interfaces of the specimen were almost

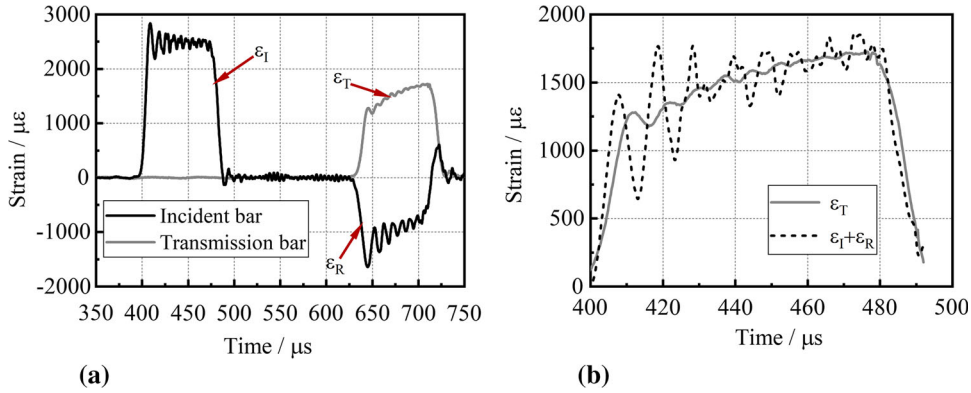

Fig. 6 Typical strain wave of Q550 at 23.6 m/s: (a) raw three-wave signals obtained from the incident bar and transmission bar in SHPB testing and (b) comparison of $\varepsilon_I + \varepsilon_R$ and ε_T

equilibrated during the test, which could be described by two equations: $F_f = EA_0(\varepsilon_I + \varepsilon_R)$ and $F_b = EA_0\varepsilon_T$, respectively. Therefore, the assumption of stress equilibrium was mainly validated, except for the beginning of SHPB tests.

b. Definition of strain rate

It is well known that most of the steels have strain-rate sensitivity. However, it is quite challenging to obtain a constant strain rate over the entire loading period for SHPB tests. Therefore, it is essential for clarifying the definition of the representative strain rate appropriately so as to characterize the strain-rate effect. Referring to (Ref 26), the average strain rate was calculated during the entire loading duration by strain-rate time histories, as shown in Fig. 7(a). It can be noted that three curves of repeated tests were almost coincident, and the mean strain rate calculated by averaging the entire strain-rate histories was determined to represent the strain rate for each impact velocity.

c. Stress–strain curves

All the results of Q550 at five different strain rates ranged from 540 to 3831 s^{-1} were obtained from the SHPB tests by Eq 1. Figure 8 demonstrates the engineering stress–strain curves for each strain rate. It can be seen that the test results of repeated experiments showed good consistency at each strain rate. The average engineering stress–strain curves were calculated from the three repeated experiment results at each strain rate, except for 540 s^{-1}. At the strain rate 540 s^{-1}, only sample 1 and sample 2 were averaged since the curve of sample 3 was apparently different compared with others. Besides, the curve at 540 s^{-1} was shorter than that at higher strain rates. The reason is that in order to get a relatively lower strain rate, the smaller gas pressure was set during the test, leading to lower impact energy. Due to the lower impact energy and relatively short strike bar in this paper, the specimen performed less deformation at lower strain rates. The true stress–strain curves were taken out by Eq 2 and were transformed into plastic stress–strain curves. The engineering, true, and true plastic stress–strain curves ware compared in Fig. 9. In particular, the descent stage of true stress–strain curves at 0.00025 s^{-1} in Fig. 9(b) and (c) was abandoned, because Eq 2 was no longer valid after necking owing to the inhomogeneous strain field and the triaxial stress state.

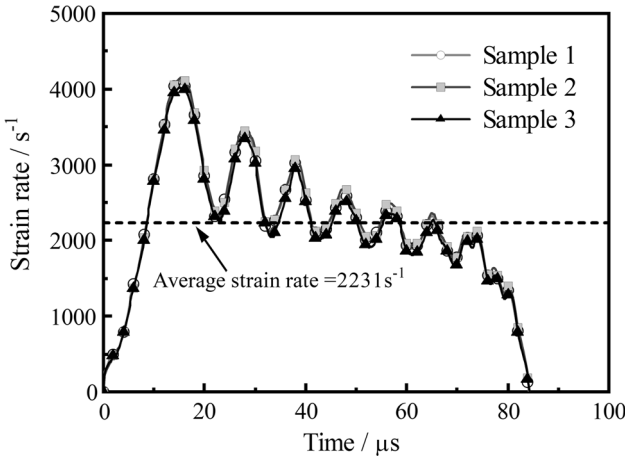

Fig. 7 Representative strain rate of Q550 steel at the impact velocity of 23.6 m/s

d. Dynamic increase factor

Based on the results from above, with the increase in strain rate, the change in the tendency of plastic strain-hardening behavior was not noticeable, but the growth of flow stress was evident. In this sense, the plastic flow stress of Q550 is strain-rate sensitive. DIF that is a general index to depict the magnitude of strain-rate hardening was introduced in this study. DIF in this paper can be expressed through dividing dynamic stress by static stress: $\mathrm{DIF} = \sigma_d/\sigma_s$, which characterizes the rate-dependence of flow stress. Therefore, the DIF was calculated according to (Ref 26) to represent the strain-rate effect of Q550 in accordance with Fig. 9(c), as listed in Table 3.

Obviously, the DIF of Q550 keeps increasing as the strain rate grows. As the strain rate reaches to 3831 s^{-1}, the DIF arrives at 1.269, while it is 1.161 at strain rate 540 s^{-1}. But the increment of DIF tends to become smaller, especially for the strain rate over 3112 s^{-1}. DIF, as the critical issue for rate-dependent models, would be discussed in detail in the following section.

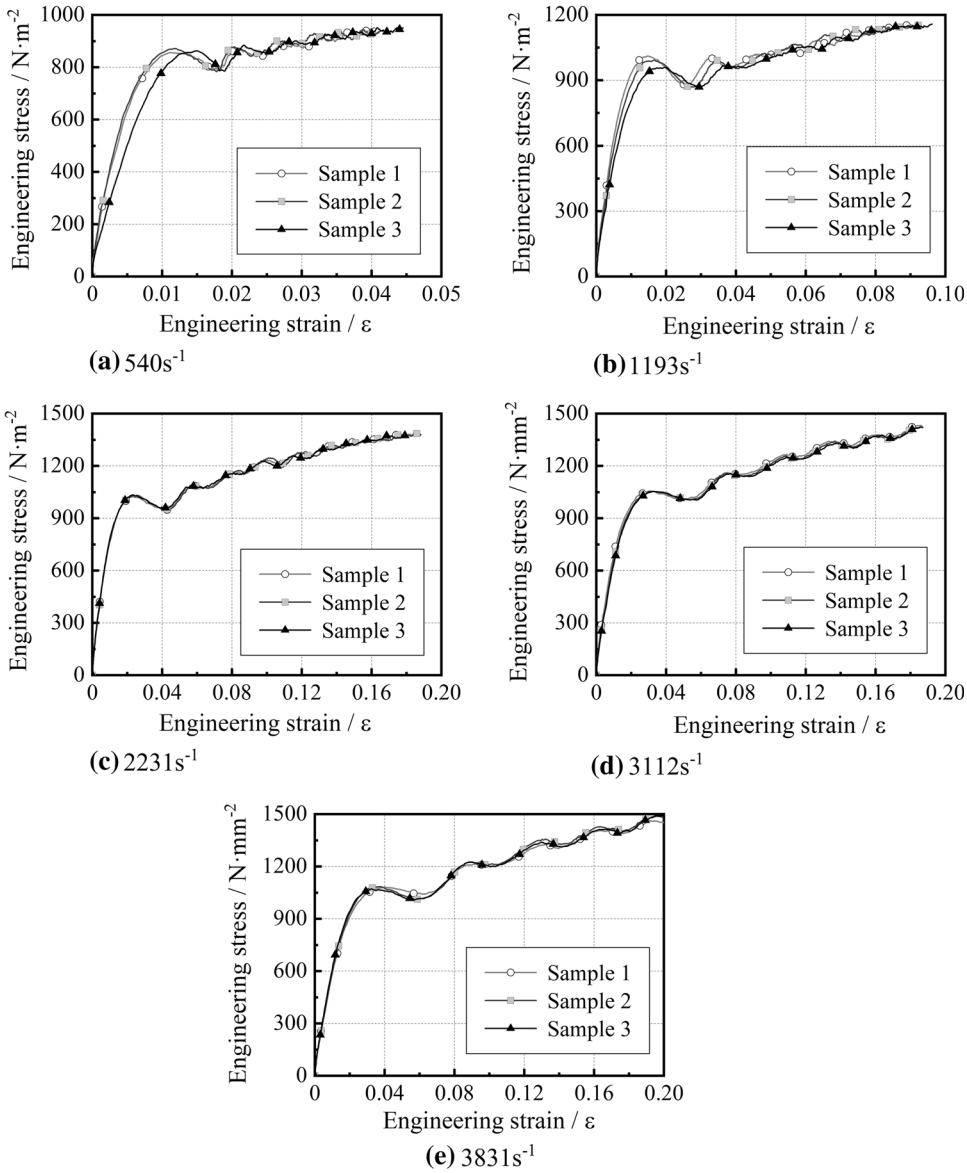

Fig. 8 Engineering stress–strain curves of Q550 in three repeated tests under different strain rates

e. Microstructure

The microstructure of Q550 steel before and after dynamic tests at different strain rates could be seen in Fig. 10. From Fig. 10(a), it shows that the microstructure of Q550 steel before the dynamic test is typical granular bainite. The white phase is ferrite matrix, and the black phase is martensite/austenite. This microstructure can be obtained after rolling and cooled in air to room temperature. Comparing other figures (i.e., Fig. 10(b), (c), (d), (e), and (f)) with Fig. 10(a), the fact is that Q550 steel has obvious deformation after dynamic tests under different strain rates. The larger the strain rate is, the more obvious the deformation is. The texture structure was formed, but there was no phase transition phenomenon. It might be attributed that under the condition of high-speed impact, although the high-speed impact increases the temperature of the samples, it has not yet reached the phase transition point.

The microstructure at the edge of samples for Q550 steel before and after dynamic tests at different strain rates is shown in Fig. 11. Comparing Fig. 11 with Fig. 10, the deformation texture at the edge of the sample is more obvious than that of the center, which is attributed to that there is no constraint limit at the edge. The traces of plastic flow could also be found in Fig. 11(d), but no phase transition has been observed.

3.2 Constitutive Models

For evaluating the performance of structures or components subjected to impact, blast, and progressive collapse, those real and accurate constitutive models describing the mechanical properties of materials subjected to such dynamic loadings are required. A series of constitutive models have been developed in the past decades, which are used to describe the strain-rate effect of materials for the use of theoretical and numerical finite element analyses. Among them, Johnson–Cook (J–C) model (Ref 32) and Cowper–Symonds (C–S) model (Ref 33) are popularly and frequently utilized by scholars to analyze the materials or structures subjected to those dynamic loadings, owing to their simplicity and practicability.

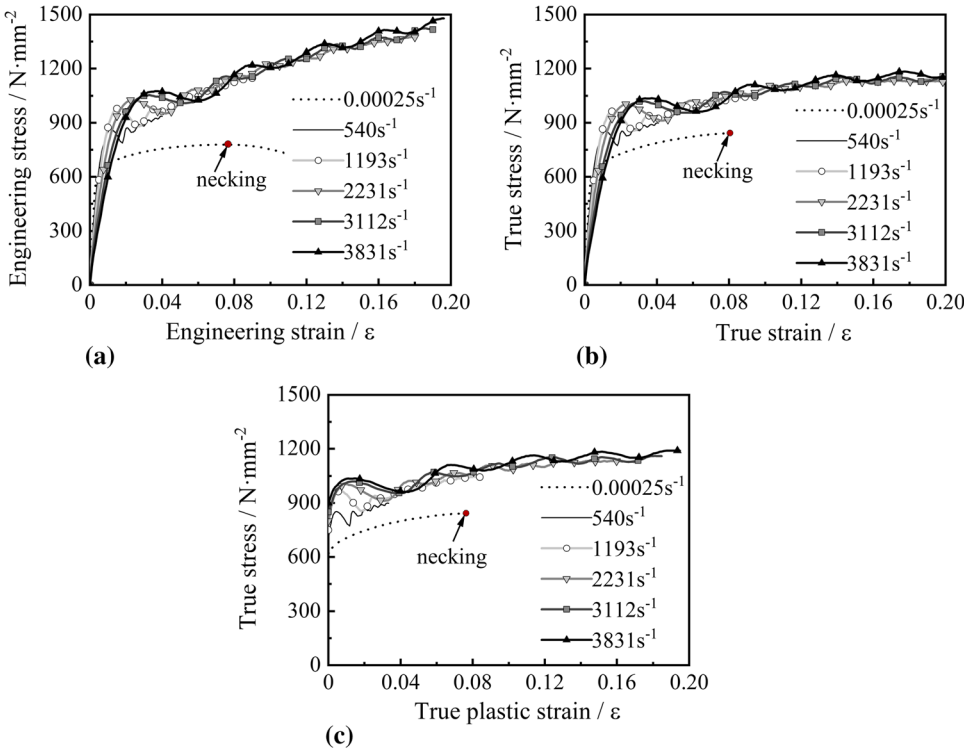

Fig. 9 Comparison of (a) engineering, (b) true, and (c) true plastic stress–strain curves for Q550 under various strain rates from 0.00025 to 3831 s^{-1}

Table 3 DIF of Q550 at each strain rate

Strain rate, s^{-1}	540	1193	2231	3112	3831
DIF	1.161	1.208	1.237	1.255	1.269

3.2.1 Standard Johnson–Cook Model. J–C model as Eq 3 has been widely accepted in describing the isotropic hardening, strain-rate hardening, and thermal softening behaviors of materials, especially for metallic materials.

$$\sigma = (A + B\varepsilon^n)(1 + C\ln\dot{\varepsilon}^*)(1 - T^{*m}) \quad \text{(Eq 3)}$$

where σ and ε are the plastic stress and plastic strain, respectively; $\dot{\varepsilon}^* = \dot{\varepsilon}/\dot{\varepsilon}_0$ $(\dot{\varepsilon}_0 = 0.00025s^{-1})$; $T^* = (T - T_r)/(T_m - T_r)$, T, T_r, and T_m are the test, room, and melting temperature, respectively. *A, B, C, m,* and *n* are the material coefficients.

All SHPB specimens were tested at room temperature, so $T^* = 0$. Then, the J–C model can be expressed as Eq 4:

$$\sigma = (A + B\varepsilon^n)(1 + C\ln\dot{\varepsilon}^*) \quad \text{(Eq 4)}$$

The standard J–C model would not consider the coupling effects of isotropic strengthening, strain-rate hardening of materials. Figure 9(c) shows that Q550 steel had experienced strain hardening phenomena with the increase in plastic strain at high strain rates, which was similar to that under a quasi-static test. So, the stress–strain curves of Q550 at high strain rates could be described by multiplying the quasi-static curve by a magnification factor (DIF).

Firstly, for the quasi-static experiments as $\dot{\varepsilon}^* = 1$, Eq 4 could be simplified and expressed as $\sigma = A + B\varepsilon^n$, where A refers to the yield stress at quasi-static conditions, while B and n refer to strain-hardening effect, which can be obtained by fitting the stress–strain curves of the quasi-static experiments. As a result, A was taken as 624 MPa, B was 850 MPa, and n was 0.51 in this study. A good fit for the stress–strain curve between the tests and the fitted J–C model can be seen clearly in Fig. 12(a).

After that, the value of C can be fitted based on the SHPB experimental results through Eq 5:

$$\frac{\sigma}{\sigma_s} - 1 = C\ln\frac{\dot{\varepsilon}}{\dot{\varepsilon}_0} \quad \text{(Eq 5)}$$

where $\sigma_s = A + B\varepsilon^n$, which is the quasi-static flow stress, and σ represents the dynamic flow stress in accordance with the SHPB test data.

For the J–C model, C is the essential parameter that characterizes the strain-rate effect, so its value is crucial to determine the stress–strain relationship for materials at high strain rates. Over the past years, researchers have studied the dynamic behaviors of mild steels and suggested some values of C describing the strain-rate effect. For example, the J–C models with $C = 0.076$ $(\dot{\varepsilon}_0 = 1s^{-1})$ (Ref 34) fitted for a type of mild steel with the yield strength of 217 MPa and $C = 0.0331$ $(\dot{\varepsilon}_0 = 0.001s^{-1})$ (Ref 24) for Q345 structural steel, respectively, were proposed. However, the J–C models might overestimate the dynamic stress for Q550 by over 20%, if either of C was used to predict the DIF of Q550 directly, as shown in Table 4.

In this study, five different strain rates were employed to test the dynamic responses of Q550 and all DIFs at each strain rate from 540 to 3831 s^{-1} were also determined (Table 3). Each

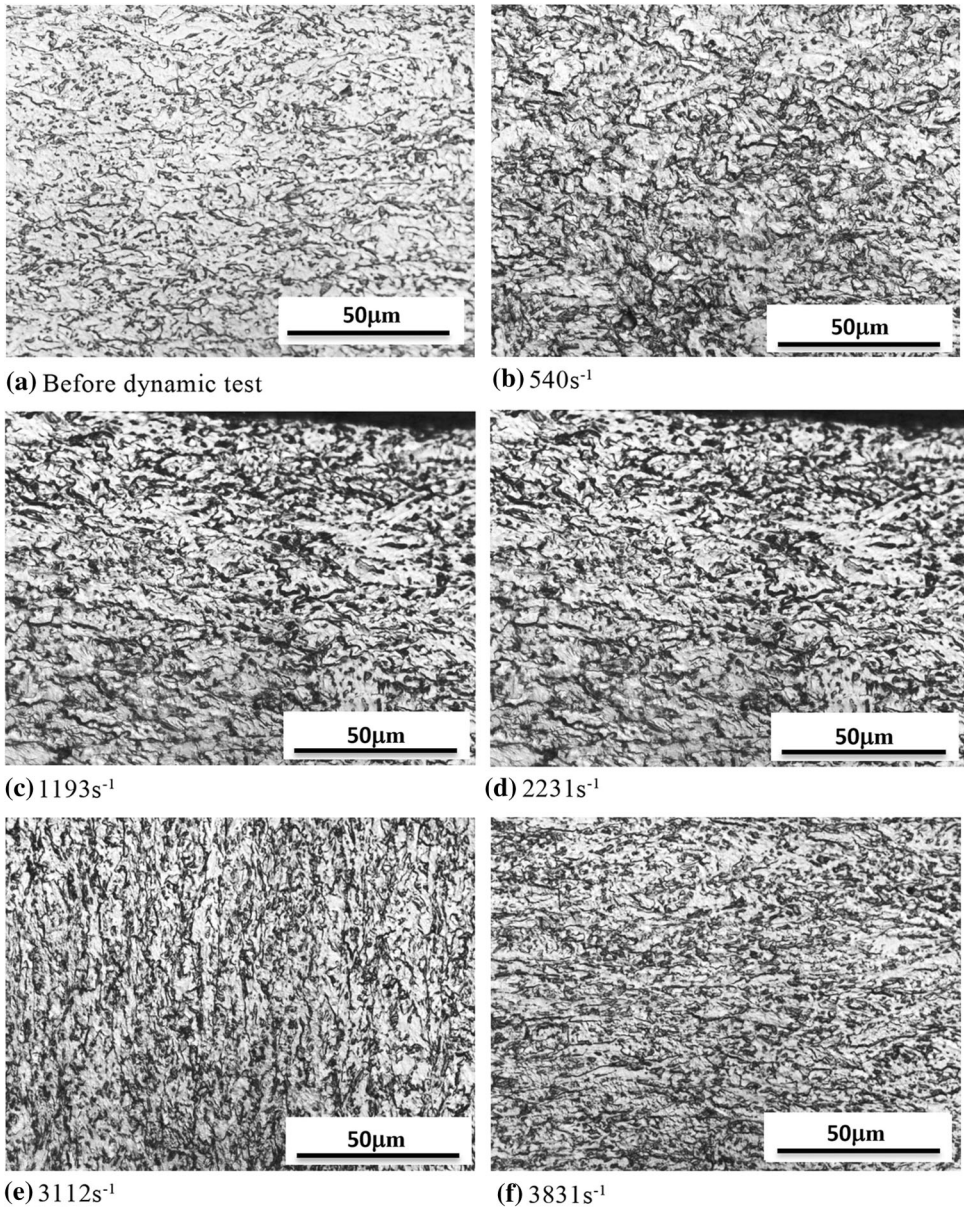

Fig. 10 Microstructure of Q550 steel before and after dynamic tests at different strain rates

DIF was chosen to fit the parameter C by Eq 5, and the relationship of value C versus strain rate is represented in Fig. 13. As a result, C was taken as 0.014 on average.

In order to estimate the accuracy of the developed standard J–C model, the flow stress versus true plastic strain interpolated from it and the original test results at each strain rate were compared, as shown in Fig. 12. It can be seen apparently that the standard J–C model assuming $C = 0.014$ is basically in good agreement with the test curves.

It should be noticed that because the values of parameters A, B, and n were obtained according to the quasi-static tension tests for Q550 in this paper, these values can be replaced by fitting the tensile curves for other similar grades of steels if necessary. However, due to the uncoupling effects of strain hardening and strain-rate increase in the J–C model, the strain-rate coefficient C may still provide a reference for other related research.

3.2.2 Modified Johnson–Cook Model. The standard J–C model with suggested material coefficients in this paper overrated the flow stress slightly at 540 s^{-1}, but underrated the flow stress when the strain rate was over 3112 s^{-1}. It is because that value of C was a constant in standard J–C model obtained on average from the test results. Actually, the value of C increased with the growth of strain rate, which had 22.5 and 14.1% deviation from the mean value for the strain rate

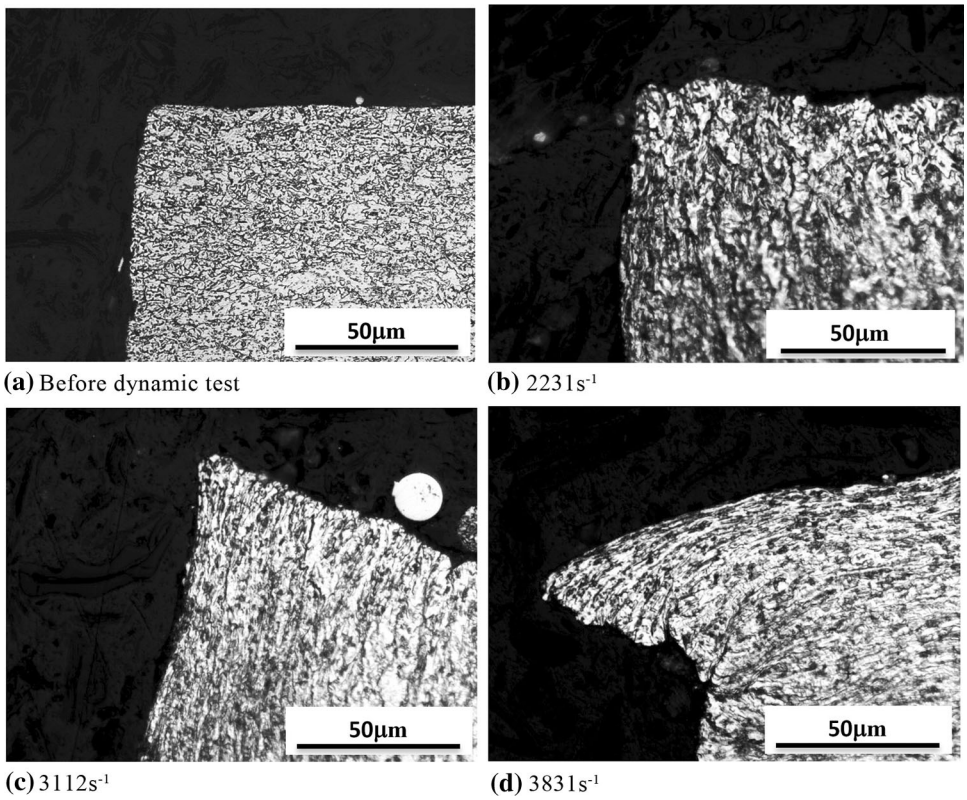

(a) Before dynamic test (b) 2231s^{-1}

(c) 3112s^{-1} (d) 3831s^{-1}

Fig. 11 Microstructure at the edge of samples for Q550 steel before and after dynamic tests

540 and 3831 s^{-1}, respectively, as shown in Fig. 13. Therefore, the method that using a single value at a single strain rate or averaging all values for C could be optimized. Optimizing the prediction accuracy of J–C model, the constant C would be described as a power function of strain rate $C(\dot{\varepsilon})$, which was in better agreement with the tendency of the increase in C with strain rate. Hence, $C = 0.014$ would be substituted by $C = 0.0034\dot{\varepsilon}^{0.19}$, and then, a new modified J–C model has been proposed. Figure 12 also shows a comparison between the prediction of the modified J–C model and the tests. Though similar prediction accuracy could be generally obtained by using the modified J–C model, the benefits might be seen when a low or high strain rate is applied, which is shown in Fig. 14. It is suggested when the strain rate is moderate or for simplification, the standard J–C model has acceptable accuracy; otherwise, the modified J–C model may be a better choice.

For verification, the test results of Q550 were compared with various models as shown in Fig. 14. As mentioned in Table 4, the previous J–C models (Ref 24, 34) based on normal-strength mild steels overestimated the DIF by 20%, which is also shown in Fig. 14(a). Besides, the models (Ref 28, 30) obtained from high-strength steel bars covering the strength up to 710 MPa were employed to predict the DIF of Q550, and the test data of high-strength steel with the yield stress of 631 MPa as well as the developed model in (Ref 31) were also added into the comparison as shown in Fig. 14(b). Note that among the models, the modified J–C model suggested in this study exhibited higher accuracy for the tests from this paper. It also had an acceptable agreement with the 631 MPa steel at intermediate strain rates.

3.2.3 Cowper–Symonds Model. The Cowper–Symonds model is another dynamic constitutive model describing the strain-rate dependence of the material. Not only is the C–S model intuitive and straightforward, but it can describe the DIF of flow stress precisely for most materials in terms of dynamical analyses. It is, therefore, another widely accepted model by scholars and engineers to represent the rate-dependent change of the dynamic flow stress. The standard C–S model is expressed by Eq 6.

$$\frac{\sigma}{\sigma_s} = 1 + \left(\frac{\dot{\varepsilon}}{D}\right)^{1/p} \quad \text{(Eq 6)}$$

where σ_s and σ refer to the quasi-static flow stress and the dynamic flow stress with the strain rate of $\dot{\varepsilon}$, respectively. D and p are the material constants, fitted by Eq 7 in logarithmic coordinates.

$$\ln(\dot{\varepsilon}) = p\ln\left(\frac{\sigma_d}{\sigma_s} - 1\right) + \ln(D) \quad \text{(Eq 7)}$$

Over the past decades, C–S models with suggested coefficients have been worked out by researchers. Among them, an

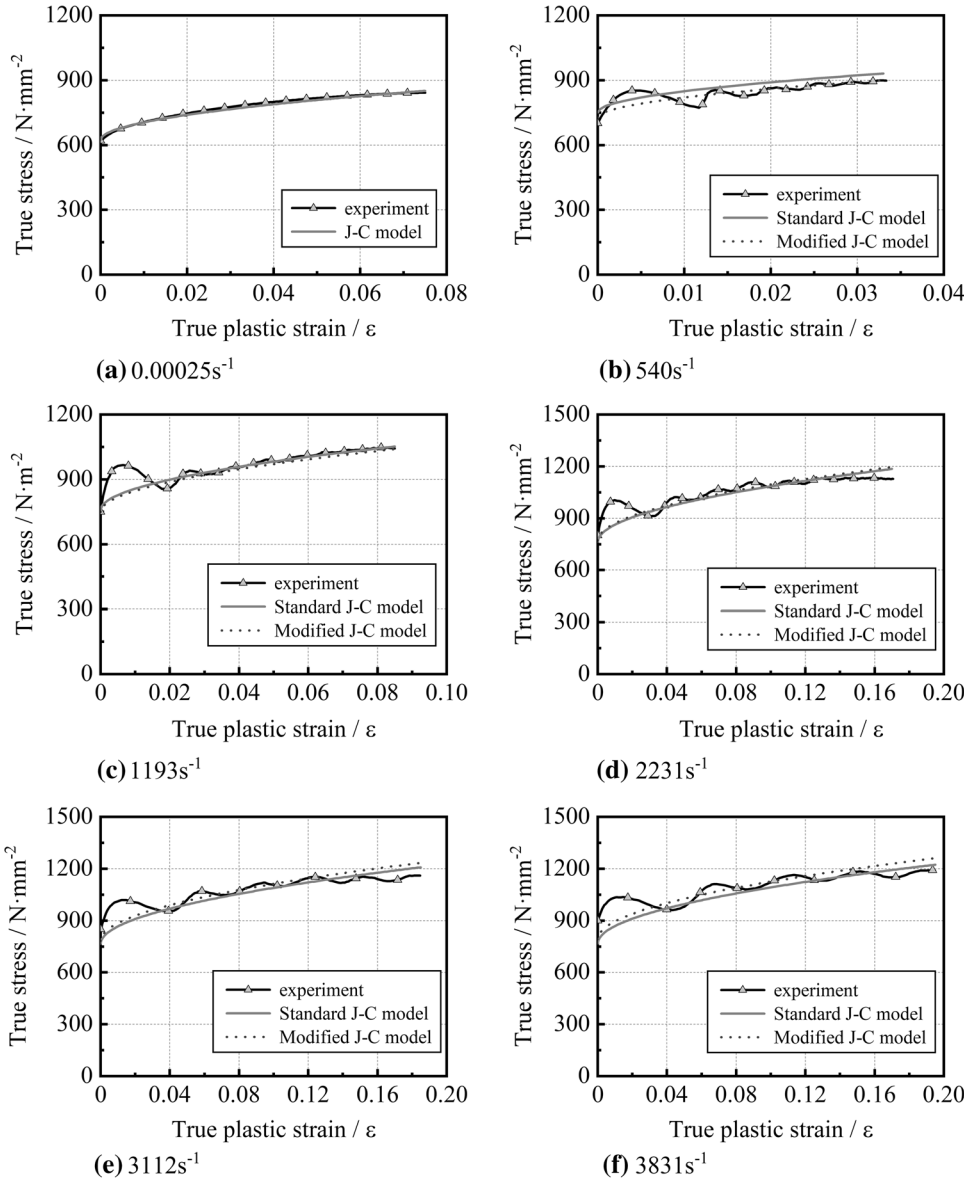

Fig. 12 Comparison among the experimental results, standard J–C model, and modified J–C model for Q550 at each strain rate

Table 4 Comparisons of DIF for Q550 under each strain rate with different J–C models and C–S models

		J–C model				C–S model		
$\dot{\varepsilon}$, s^{-1}	Test	Ref 34	Ref 24	$C = 0.014$	$C = 0.0034\dot{\varepsilon}^{0.19}$	Ref 35	Ref 23	$D = 550{,}000$, $p = 3.8$
540	1.161	1.478 (27)	1.437 (24)	1.204 (4)	1.164 (0)	2.680 (131)	1.440 (24)	1.162 (0)
1193	1.208	1.538 (27)	1.463 (21)	1.215 (1)	1.201 (− 1)	2.968 (146)	1.590 (32)	1.199 (− 1)
2231	1.237	1.586 (28)	1.484 (20)	1.224 (− 1)	1.235 (0)	3.231 (161)	1.744 (41)	1.235 (0)
3112	1.255	1.611 (28)	1.495 (19)	1.229 (− 2)	1.256 (0)	3.384 (170)	1.842 (47)	1.256 (0)
3831	1.269	1.627 (28)	1.502 (18)	1.232 (− 3)	1.270 (0)	3.485 (175)	1.910 (51)	1.271 (0)

The values in parentheses indicate the deviation in percentage between the predicted value and the test data of DIF. For instance, the value 1.478(27) at 540 s^{-1} predicted by (Ref 34) refers to $(1.478 - 1.161)/1.161 \times 100\% = 27\%$

empirical C–S model with the widely used material parameters: $D = 40.4$ and $p = 5$ for mild steels was fitted experimentally for predicting the DIF of yield stress (Ref 35). Besides, another empirical C–S model with experimentally fitted parameters: $D = 4945$ and $p = 2.696$ for S355 steel (Ref 23) was also obtained. As mentioned before, no model has been established to predict the DIF of Q550. If the C–S model with the aforementioned values for D and p was adopted for calculating the DIF of Q550, the deviations in percentage between its predicted values and measured values were more than 130 and 25%, respectively, as shown in Table 4 and Fig. 14(a). Therefore, the existing models could not be directly applied for Q550, with large overestimations for its strain-rate effect.

For this paper, the C–S model was suggested by fitting the DIF of Q550 at strain rates through Eq 7. So, $D = 550{,}000$ and $p = 3.8$, according to the fitting data in logarithmic coordinates based on the experiment results. Figure 14 shows that the present fitted C–S model with two new material constants has satisfactory predicting accuracy for Q550, which is almost the same as the modified J–C model.

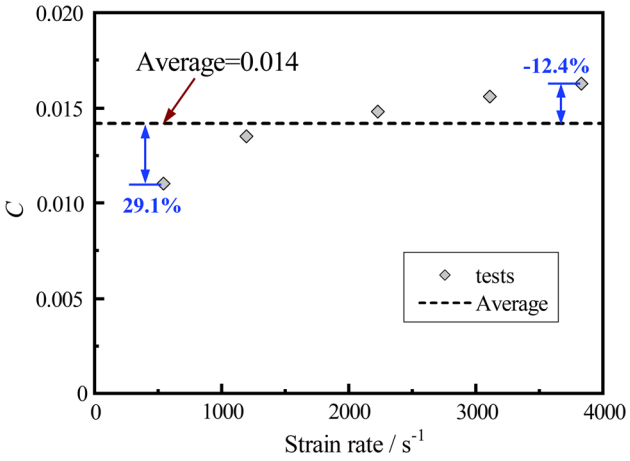

Fig. 13 Relationship of C vs. strain rate

4. Conclusions

In this study, Q550, a grade of HSSS, has been investigated systematically both under quasi-static and dynamic SHPB tests with the strain rate from 0.00025 to 3831 s^{-1}. Following conclusions may be drawn according to the study:

(1) Q550 showed an apparent strain-rate sensitivity on strength. As the strain rate increased to 3831 s^{-1}, flow stress also grew, and the DIF arrived at 1.269. However, the tendency of strain hardening was almost the same as that of the quasi-static tests even if it was under high-speed loadings.

(2) Compared with normal mild steel, Q550 performed less strain-rate sensitivity by over 20%. The existing models obtained from normal mild steel were not suggested to be directly applied to predicting the dynamic properties of Q550, which would overrate its strain-rate effect.

(3) The parameters of the standard J–C model were reported, and its ability in fitting stress–strain curves of Q550 was demonstrated. Particular attention on the strain-rate parameter C was paid in this study, and the value of C has been analyzed deeply. Both a constant of 0.014 for the standard J–C model and a rate-dependent parameter $C = 0.0034\dot{\varepsilon}^{0.19}$ in a modified J–C model were suggested. A new C–S model with two material coefficients: $D = 550{,}000$ and $p = 3.8$ was also suggested by fitting the DIF of Q550 at different strain rates.

(4) The models suggested in the paper performed higher prediction accuracy for Q550 or other similar strength structural steel at strain rates up to 3831 s^{-1}, and they can be employed in practice for those analyses and designs of steel structures against dynamic loads (e.g., earthquake, vehicle impact, and explosion).

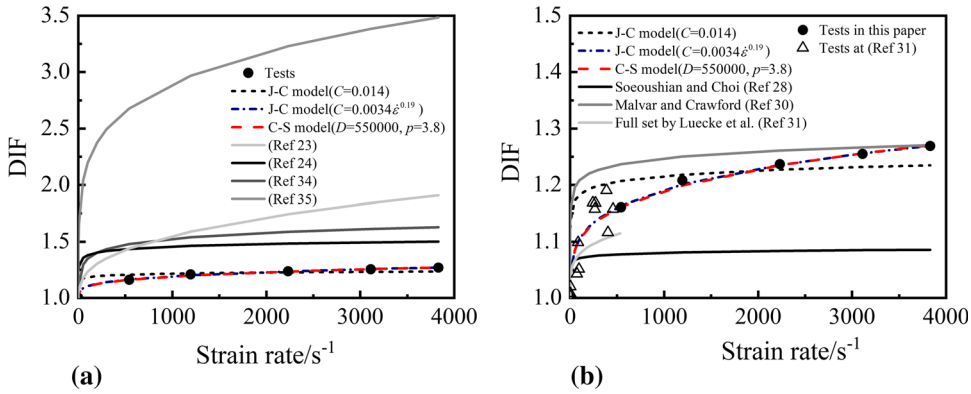

Fig. 14 Comparison of test data and various models: (a) compared with previous J–C and C–S models and (b) compared to prior models based on high-strength steels

Acknowledgments

The authors are grateful for the financial support from National Natural Science Foundation of China (Grant No. 51678194). This work is also supported by China Scholarship Council (Grant No. 201706120260).

References

1. G. Li, H. Lyu, and C. Zhang, Post-fire Mechanical Properties of High Strength Q690 Structural Steel, *J. Constr. Steel Res.*, 2017, **132**, p 108–116
2. R. Bjorhovde, Performance and Design Issues for High Strength Steel in Structures, *Adv. Struct. Eng.*, 2010, **13**(3), p 403–411
3. H.Y. Ban and G. Shi, A Review of Research on High-strength Steel Structures, *Proc. Inst. Civ. Eng. Struct. Build.*, 2018, **171**(8), p 625–641
4. L. Zhang, Y. Li, J. Wang, and Q. Jiang, Effect of Acicular Ferrite on Cracking Sensibility in the Weld Metal of Q690 + Q550 High Strength Steels, *ISIJ Int.*, 2011, **51**(7), p 1132–1136
5. A.M.P. Jesus, R. Matos, B.F.C. Fontoura, C. Rebelo, L.S. Da Silva, and M. Veljkovic, A Comparison of the Fatigue Behavior Between S355 and S690 Steel Srades, *J. Constr. Steel Res.*, 2012, **79**, p 140–150
6. H.C. Ho, X. Liu, K.F. Chung, A.Y. Elghazouli, and M. Xiao, Hysteretic Behaviour of High Strength S690 Steel Materials Under Low Cycle High Strain Tests, *Eng. Struct.*, 2018, **165**, p 222–236
7. C. Fang, X. Meng, Q. Hu, F. Wang, H. Ren, H. Wang et al., TANDEM and GMAW Twin Wire Welding of Q690 Steel Used in Hydraulic Support, *J. Iron. Steel Res. Int.*, 2012, **19**(5), p 79–85
8. J. Yan, J.Y.R. Liew, M. Zhang, and J. Wang, Mechanical Properties of Normal Strength Mild Steel and High Strength Steel S690 in Low Temperature Relevant to Arctic Environment, *Mater. Des.*, 2014, **61**, p 150–159
9. J. Chen, B. Young, and B. Uy, Behavior of High Strength Structural Steel at Elevated Temperatures, *J. Struct. Eng.*, 2006, **132**(12), p 1948–1954
10. X. Qiang, F.S.K. Bijlaard, and H. Kolstein, Post-fire Mechanical Properties of High Strength Structural Steels S460 and S690, *Eng. Struct.*, 2012, **35**, p 1–10
11. L. Kang, M. Suzuki, H. Ge, and B. Wu, Experiment of Ductile Fracture Performances of HSSS Q690 after a Fire, *J. Constr. Steel Res.*, 2018, **146**, p 109–121
12. H. Ban, G. Shi, Y. Shi, and Y. Wang, Overall Buckling Behavior of 460 MPa High Strength Steel Columns: Experimental Investigation and Design Method, *J. Constr. Steel Res.*, 2012, **74**, p 140–150
13. Y. Wang, G. Li, S. Chen, and F. Sun, Experimental and Numerical Study on the Behavior of Axially Compressed High Strength Steel Columns with H-section, *Eng. Struct.*, 2012, **43**, p 149–159
14. T. Li, G. Li, S. Chan, and Y. Wang, Behavior of Q690 High-strength Steel Columns: Part 1: Experimental Investigation, *J. Constr. Steel Res.*, 2016, **123**, p 18–30
15. T. Li, S. Liu, G. Li, S. Chan, and Y. Wang, Behavior of Q690 High-Strength Steel Columns: Part 2: Parametric Study and Design Recommendations, *J. Constr. Steel Res.*, 2016, **122**, p 379–394
16. J. Wang, S. Afshan, and L. Gardner, Axial Behavior of Prestressed High Strength Steel Tubular Members, *J. Constr. Steel Res.*, 2017, **133**, p 547–563
17. M.J. Manjoine, The Influence of Rate of Strain and Temperature on the Yield Stresses of Mild Steel, *J. Appl. Mech.*, 1944, **11**, p A-211
18. W.L. Cowell, Dynamic Tests on Selected Structural Steels. No. Ncel-Tr-642, Naval Civil Engineering Lab Port Hueneme Calif, 1969
19. R.L. Woodward and R.H. Brown, Dynamic Stress–Strain Properties of a Steel and a Brass at Strain Rates up to 104 per Second, *Proc. Inst. Mech. Eng.*, 1975, **189**(1), p 107–115
20. M.M. Haque and M.S.J. Hashmi, Stress–Strain Properties of Structural Steel at Strain Rates of up to 105 per Second at Sub-zero, Room and High Temperatures, *Mech. Mater.*, 1984, **3**(3), p 245–256
21. W. Yu, J. Zhao, and J. Shi, Dynamic Mechanical Behaviour of Q345 Steel at Elevated Temperatures: Experimental Study, *Mater. High Temp.*, 2010, **27**(4), p 285–293
22. M. Mirmomeni, A. Heidarpour, X. Zhao, C.R. Hutchinson, J.A. Packer, and C. Wu, Mechanical Properties of Partially Damaged Structural Steel Induced by High Strain Rate Loading at Elevated Temperatures—An Experimental Investigation, *Int. J. Impact Eng.*, 2015, **76**, p 178–188
23. D. Forni, B. Chiaia, and E. Cadoni, Strain Rate Behaviour in Tension of S355 Steel: Base for Progressive Collapse Analysis, *Eng. Struct.*, 2016, **119**, p 164–173
24. J. Chen, W. Shu, and J. Li, Constitutive Model of Q345 Steel at Different Intermediate Strain Rates, *Int. J. Steel Struct.*, 2017, **17**(1), p 127–137
25. J. Chen, J. Li, and Z. Li, Experiment Research on Rate-Dependent Constitutive Model of Q420 Steel, *Constr. Build. Mater.*, 2017, **153**, p 816–823
26. X. Yang, H. Yang, and S. Zhang, Rate-Dependent Constitutive Models of S690 High-strength Structural Steel, *Constr. Build. Mater.*, 2019, **198**, p 597–607
27. N.R.N. Rao, M. Lohrmann, and L. Tall, Effect of Strain Rate on the Yield Stress of Structural Steel, *ASTM J. Mater.*, 1966, **1**(1), p 684–737
28. P. Soroushian and K. Choi, Steel Mechanical Properties at Different Strain Rates, *J. Struct. Eng.*, 1987, **113**(4), p 663–672
29. M. Kassar and W. Yu, Effect of Strain Rate on Material Properties of Sheet Steels, *J. Struct. Eng.*, 1992, **118**(11), p 3136–3150
30. L.J. Malvar and J.E. Crawford, *Dynamic Increase Factors for Steel Reinforcing Bars, 28th Department of Defence Explosive Safety Board Seminar*, Orlando, USA, 1998
31. W.E. Luecke, J.D. McColskey, C.N. McCowan, S.W. Banovic, R.J. Fields, T.J. Foecke et al., *Mechanical Properties of Structural Steels—Federal Building and Fire Safety Investigation of the World Trade Center Disaster (NIST NCSTAR 1-3D), Gaithersburg*, National Institute of Standard and Technology, USA, 2005
32. G.R. Johnson and W.H. Cook, A Constitutive Model and Data for Metals Subjected to Large Strains, High Strain Rates and High Temperatures, Proceedings of the 7th International Symposium on Ballistics, Den Haag, The Netherlands, 1983
33. G. Cowper and P.S. Symonds, Strain Hardening and Strain Rate Effects in the Impact Loading of the Cantilever Beams, Technical Report 28, Providence, RI: Brown University, Division of Applied Mathematics, 1957
34. K. Vedantam, D. Bajaj, N.S. Brar, and S. Hill, Johnson–Cook Strength Models for Mild and DP 590 Steels, *AIP Conf. Proc.*, 2006, **845**(1), p 775–778
35. N. Jones, Structural Aspects of Ship Collisions, *Structural Crashworthiness*, N. Jones and T. Wierzbicki, Ed., Butterworths, London, 1983, p 308–337